Optimization Method for Isodensity Surface Models Obtained with Electron Microscope Tomography Data

D. Ress, M. L. Harlow, R. M. Marshall, U. J. McMahan

Department of Neurobiology, Stanford University Medical School, CA, USA

Abstract—**Electron microscope tomography produces reconstructed biological tissue volumes containing structural data with few-nanometer spatial resolution. Frequently, surface models are constructed to visualize and analyze the structural data. These models are usually constructed to approximate the contrast boundaries of various structural components within the volume. An automatic method is presented for obtaining isodensity surface models that correspond most closely to the steepest contrast boundary at the edge of each component. We validate our method using simulated volumetric data, and demonstrate its application to a reconstructed volume obtained from the neuromuscular junction of the frog.**

Keywords—**tomography, segmentation, ultrastructure, optimization, electron microscopy**

I. INTRODUCTION

The best spatial resolution for studying the shapes and organization of subcellular components in biological tissues is obtained in 3D reconstructions of heavy-metal stained tissue samples generated by electron microscope tomography [1-6]. Particularly high-resolution information (2—3 nm) was obtained from the active-zone material found at the neuromuscular junction of the frog, using an analysis method based on segmentation of individual volumes-of-interest (VOIs), followed by construction of an isodensity surface to model the structure contained with the VOI [5]. The isodensity level of these surfaces was adjusted by a human operator to produce a surface model that visually appeared to provide a best fit to the contrast boundary at the edge of the structure contained in the VOI.

We present a new method to automatically determine an optimal isodensity level for each surface model. The isodensity level is chosen to maximize the local spatial gradients in the vicinity of the isodensity contour. The new method offers several advantages. It provides an objective method to obtain an accurate surface model, and it is faster and more convenient than visually guided manual methods [7-10], thus reducing operator time and effort.

II. METHODOLOGY

Individual components of the reconstructed volume are first segmented to form VOIs that contain but do not precisely delineate their boundaries [5]. Isodensity surface models are then constructed using only the contents of each VOI.

An initial isodensity level is chosen using the cumulative distribution function for gray values within the VOI. Specifically, we select the value that most closely corresponds to that enclosing 60% of the darkest voxels within the isodensity surface. This initial surface provides what is usually a structurally reasonable starting point for the optimization.

A spatial-gradient quality metric, M, is then calculated for the surface. At each vertex on the surface, the local vector spatial gradient, $\vec{\nabla}G$, is calculated by convolving the gray-scale data in the vicinity of the vertex with $3\times3\times3$ Cartesian finite difference kernels $\mathbf{d}_{x, y, z}$, (For example, $\mathbf{d}_x$ consists of nine repeated rows of the vector [0.5, -1, 0.5].) Next, the outward surface-normal vector, $\hat{n}$, is calculated at each vertex, and we form the scalar product of this vector with the spatial gradient to obtain the outward-normal component of the spatial gradient. Finally, we calculate the area of the surface trapezoid associated with each vector, and form the area-weighted sum of the normal spatial gradient, a numerical approximation of:

$$M = \int dA \left(\hat{n} \bullet \vec{\nabla}G \right). \qquad (1)$$

The isodensity value of the surface is now varied in an optimization process that seeks to maximize M. We use a standard optimization routine that is implemented in the software product IDL (Research Systems Inc, Boulder, CO, USA), using a downhill-simplex method [11].

To provide an objective standard to assess the performance of the optimization method, we created a simulated volume containing realistic representations of synaptic vesicles. We chose an isotropic voxel size of 1 nm, a reasonable value for actual reconstructed EM tomography volumes. Vesicles were simulated by summing a few low-order spherical harmonics to create a spheroidal shape with roughly 50-nm diameter. To assess the ability of our surface models to delineate fine-scale structure, surface texture was created by adding additional low-amplitude, high-order spherical harmonics. Superposing two such spheroids with radii offset by 5 nm simulated the trilaminar character of stained membranes. The entire simulated volume was smoothed slightly ($3\times3\times3$ boxcar kernel, repeated twice) to reduce quantization artifacts, and normally distributed noise was added to simulate a typical signal-to-noise ratio of five.

Surface models were also obtained from actual data from the frog neuromuscular junction. Our preparations were conventional [12, 13]. Briefly, cutaneous pectoris muscles of adult *Rana pipiens* (5 cm nose rump length) were, in sequence, fixed with 1% phosphate buffered glutaraldehyde, refixed and stained with 1% osmium tetroxide in phosphate

buffer, stained with saturated aqueous uranyl acetate, dehydrated in ethanol and propylene oxide and embedded in Epon 812. Thin sections having a silver interference color (~50 nm thick) were mounted on 1×2 mm single slot Formvar coated grids, and stained with uranyl acetate followed by lead citrate. For use in the alignment of tilt images, mounted sections were floated on a drop of ~ 0.01% unconjugated gold colloid in H_2O (Sigma Chemical Co, St Louis, MO) for 1—2 min and air-dried.

The data set was made at room temperature on a FEI Tecnai T20 electron microscope operated at 200KV. It was equipped with LaB_6 electron source, a cryoholder and a 1024×1024 CCD. The tilt series consisted of 201 images spanning angles from -75° to +75° in 0.75° increments. The images were made at a microscope magnification of 29,000×, yielding a pixel size of 0.59 nm in the image.

The gold beads on the section served as fiducial markers for aligning the tilt images. We used an alignment scheme previously developed in our laboratory [12] that provided an accuracy of 2.1 pixels (1.2 nm) RMS. Volume reconstructions were produced by weighted backprojection, and this volume was then downsampled 2× to reduce computational load.

Vesicles were segmented from the reconstructed volume using a semi-automatic method applied to a series of 2D slices. Segmentation was initiated by having an operator mark an anchor path on a single volume slice. This path was then automatically propagated perpendicular to the slice plane. The segmentation VOIs were somewhat larger than the stained structures that they enclosed to allow accurate and complete isodensity-surface calculations [5].

III. Results

A. Simulated synaptic vesicle

Surface models were generated and optimized for a simulated volume containing several vesicles and some simple cylindrical structures that simulate active-zone material. Here, we present the results of optimizing the isodensity surface model for one of the vesicles.

The default choice of isodensity level is not optimal. The blue 'x' in Fig. 1 indicates the M value of the initial choice. The optimization routine sampled the isodensity levels shown by the set of orange asterisk symbols. For reference, these points are overlaid on curve formed by calculating M on a closely sampled grid of isodensity levels.

The optimal isodensity level produces a surface model of the vesicle structure that precisely follows the detailed outline of the contrast boundaries. When the isodensity level is too low, the surface model disintegrates into multiple surfaces surrounding many small subvolumes (Figs. 2a, b). When the isodensity level is too high, the surface model only delineates the outer boundaries of the vesicle membrane, showing less detail on the outer surface and missing the trilaminar character of the membrane (Figs. 2c,

d). At the optimal value, both the outer and inner leaflets of the trilaminar membrane are delineated by the surface model (Figs. 2e, f).
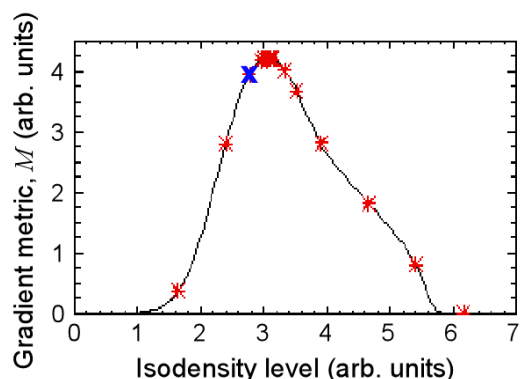

Fig. 1. Variation of spatial gradient metric with isodensity level for simulated data. Optimization started at the blue 'x,' and sampled all the points marked by the red '*' symbols.
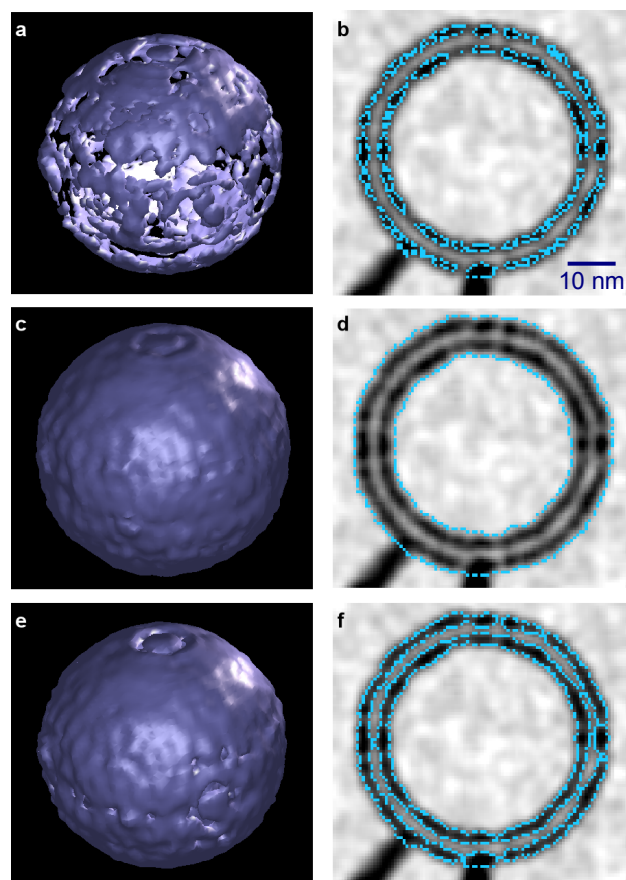

Figure 2. Example isosurface models of a synthetic synaptic vesicle. Left column shows 3D rendering; right column shows cross-section of the model (blue lines) overlaid on the grayscale data. (a, b) isodensity level too dark. (c, d) isodensity level too light. (e, f) optimal isodensity level
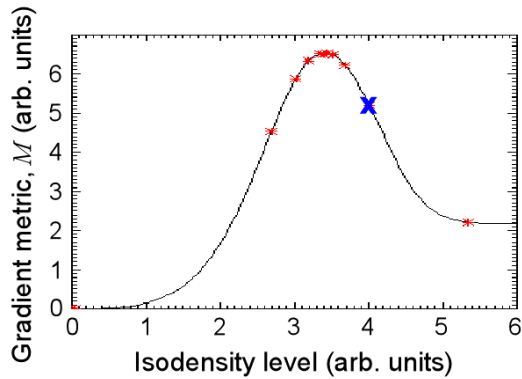
B. Actual synaptic vesicle

Figure 3. Variation of spatial gradient metric with isodensity level for biological data. (Symbols as in Fig. 1.)
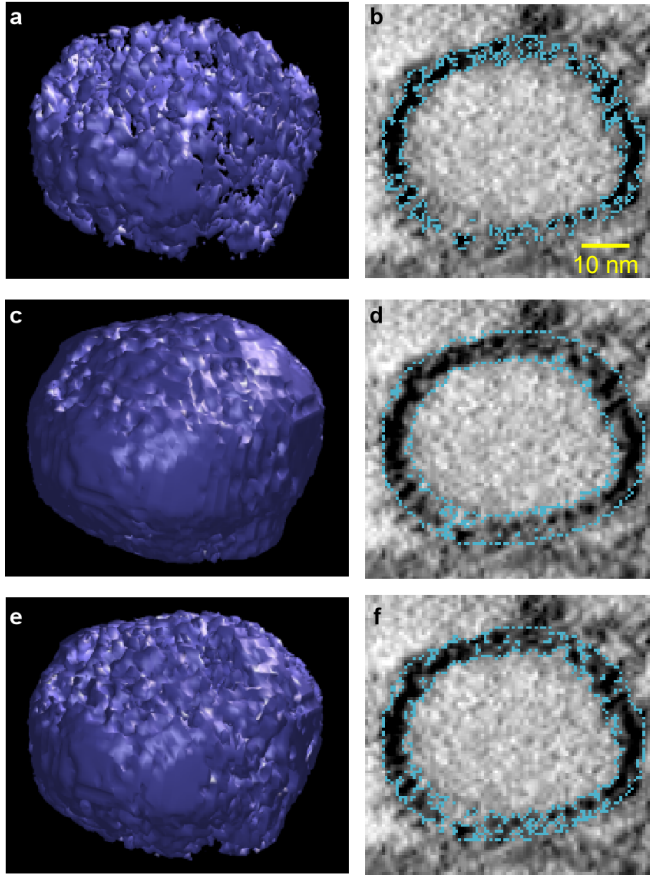

Figure 4. Example isosurface models of an actual synaptic vesicle. (a, b) isodensity level too dark. (c, d) isodensity level too light. (e, f) optimal isodensity level

Application of the optimization scheme to a synaptic vesicle obtained from a frog neuromuscular junction revealed similar behavior of the algorithm. The spatial-gradient metric shows a well-defined maximum, and the maximization algorithm samples it in a fashion similar to that of the simulated vesicle (Fig. 3).

The surface models also show a similar variation with isodensity level around the optimum. At levels that are too low, the model again disintegrates, but the greater structural complexity of the actual vesicle gives rise to a more complex collection of surfaces (Figs. 4a, b). At levels that are too high, the model surface does not follow the detailed spatial variations of the vesicle membrane (Figs. 4c, d). The optimal level appears to follow the contrast boundaries with greatest accuracy. In fact, the optimal model reveals a complex surface topography of the vesicle membrane that may result from transmembrane macromolecules that are associated with the outer and inner surfaces of the synaptic vesicle membrane [14].

IV. Discussion

We used a particular quality metric for the isodensity surface, the area-weighted sum of the normal spatial gradient, because it had a smooth, well-behaved variation with isodensity level. We experimented with several other metrics, including the summed normal spatial gradient, average normal spatial gradient, and the mean-squared normal gradient. The first two methods were rejected because they behaved poorly as isodensity level was varied, exhibiting large jumps and fluctuations. The mean square gradient was rejected because it tended to give a lesser quality visual match between the isodensity surface and the contrast boundary. Adding the areal weighting improved the numerical behavior of the method by de-emphasizing small regions of particularly large or small spatial gradients in the vicinity of a surface model. The areal weighting forces the fitting procedure toward larger-area surface models, avoiding the tendency of other optimization metrics to collapse upon small regions of large spatial gradients.

The surface produced at the optimal isodensity level accurately follows the contrast boundary at the edge of a stained structural component. In simulated data, the optimal surface delineated the two leaflets of a trilaminar membrane. In actual data, the optimal surface delineated a more complex topography they should be of biological interest. In general, our optimization procedure provides an isodensity surface model that maximizes accuracy and reliability, providing topographic data at the full resolution of the reconstructed volume.

It should be emphasized, however, that there is no one ideal choice of isodensity surface model for this volumetric data. For example, if one wanted to generate a surface encompassing the full thickness of a trilaminar membrane, it would be appropriate to use a larger (lighter) isodensity level than would be obtained by the optimization described here. Nevertheless, the optimization process is particularly

attractive because it provides an objective starting point for the generation of surface models. Modified isodensity levels necessary for specialized applications, such as example described above, can be obtained by modifying the optimal isodensity level in a standardized fashion, for example by applying a fixed multiplicative offset.

V. CONCLUSION

We have presented a procedure to determine the isodensity level for a surface model fit to volume-of-interest data obtained by electron microscope tomography. The method automatically determines an isodensity level that puts the surface model at the contrast boundary between a darker object and its lighter background. This isodensity level is obtained by maximizing the area-weighted moment of the normal component of grayscale spatial gradient. The optimization process greatly improves the objectivity, accuracy, and convenience of surface model generation.

REFERENCES

[1] D. Lenzi, J. W. Runyeon, J. Crum, M. H. Ellisman, and W. M. Roberts, "Synaptic vesicle populations in saccular hair cells reconstructed by electron tomography," *J Neurosci*, vol. 19, pp. 119-32, 1999.

[2] W. Baumeister, R. Grimm, and J. Walz, "Electron tomography of molecules and cells," *Trends Cell Biol*, vol. 9, pp. 81-5, 1999.

[3] M. Moritz, M. B. Braunfeld, J. C. Fung, J. W. Sedat, B. M. Alberts, and D. A. Agard, "Three-dimensional structural characterization of centrosomes from early Drosophila embryos," *J Cell Biol*, vol. 130, pp. 1149-59, 1995.

[4] M. S. Ladinsky, D. N. Mastronarde, J. R. McIntosh, K. E. Howell, and L. A. Staehelin, "Golgi structure in three dimensions: functional insights from the normal rat kidney cell," *J Cell Biol*, vol. 144, pp. 1135-49, 1999.

[5] M. L. Harlow, D. Ress, A. Stoschek, R. M. Marshall, and U. J. McMahan, "The architecture of active zone material at the frog's neuromuscular junction," *Nature*, vol. 409, pp. 479-84, 2001.

[6] B. F. McEwen, M. Radermacher, C. L. Rieder, and J. Frank, "Tomographic three-dimensional reconstruction of cilia ultrastructure from thick sections," *Proc Natl Acad Sci U S A*, vol. 83, pp. 9040-4, 1986.

[7] J. Frank, M. Radermacher, P. Penczek, J. Zhu, Y. Li, M. Ladjadj, and A. Leith, "SPIDER and WEB: processing and visualization of images in 3D electron microscopy and related fields," *J Struct Biol*, vol. 116, pp. 190-9, 1996.

[8] J. R. Kremer, D. N. Mastronarde, and J. R. McIntosh, "Computer visualization of three-dimensional image data using IMOD," *J Struct Biol*, vol. 116, pp. 71-6, 1996.

[9] Y. Li, A. Leith, and J. Frank, "Tinkerbell--a tool for interactive segmentation of 3D data," *J Struct Biol*, vol. 120, pp. 266-75, 1997.

[10] G. A. Perkins, C. W. Renken, J. Y. Song, T. G. Frey, S. J. Young, S. Lamont, M. E. Martone, S. Lindsey, and M. H. Ellisman, "Electron tomography of large, multicomponent biological structures," *J Struct Biol*, vol. 120, pp. 219-27, 1997.

[11] W. H. Frank, et al, "Section 10.4," in *Numerical Recipes in C: The Art of Scientific Computing*, Second ed. Cambridge: Cambridge University Press, 1992.

[12] D. Ress, M. L. Harlow, M. Schwarz, R. M. Marshall, and U. J. McMahan, "Automatic acquisition of fiducial markers and alignment of images in tilt series for electron tomography," *J Electron Microsc (Tokyo)*, vol. 48, pp. 277-87, 1999.

[13] U. J. McMahan and C. R. Slater, "The influence of basal lamina on the accumulation of acetylcholine receptors at synaptic sites in regenerating muscle," *J Cell Biol*, vol. 98, pp. 1453-73, 1984.

[14] T. C. Suedhof and R. H. Scheller, "Mechanism and Regulation of Neurotransmitter Release," in *Synapses*, W. M. Cowan, T. C. Suedhof, and C. F. Stevens, Eds. Baltimore: The John Hopkins University Press, 2001, pp. 177-215.